Opt Quant Electron (2017) 49:401
https://doi.org/10.1007/s11082-017-1235-9

A tunable reflective polarization converter based on hybrid metamaterial

Zhongyin Xiao[1] · Huanling Zou[1] · Xiaoxia Zheng[1] · Xinyan Ling[1] · Lei Wang[1]

Received: 24 July 2017 / Accepted: 7 November 2017 / Published online: 11 November 2017

Abstract A hybrid metamaterial converter based on a hybrid layer, a gold (Au) film and a dielectric substrate is proposed to realize linear and circular polarization conversions in the terahertz (THz) band. The hybrid layer is composed of a vanadium dioxide (VO_2) plane and I-shaped resonators. The polarization conversion ratio (PCR) above 90% is achieved in a broad band range from 2.10 to 5.03 THz under both linearly and circularly polarized waves. And, the PCR is up to near unity around the resonant frequency. Meanwhile, the metamaterial convertor is sensitive to the incident angles. Moreover, a controlled modulation characteristic can be realized by the proposed polarization converter. In addition, the physical mechanism of the polarization conversion is analyzed by the distributions of surface currents. These features pave a novel way for the broad band polarization converter and hold application in the area of sensing, THz communication and tunable polarizers.

Keywords Hybrid metamaterial · Polarization converter · Terahertz · Dynamic modulation

1 Introduction

Metamaterials (MMs) have increasingly attracted immense attention caused by their particular ability to achieve polarization conversion, absorption, and filter (Grady et al. 2013; Landy et al. 2008; Lu et al. 2011) in a wide frequency scope from the microwave to terahertz, even in the optical region. The artificial electromagnetic materials which are designed by the periodic array structures have been used for a lot of related applications including sensor (Wang et al. 2015), thermal emitters (Dyachenko et al. 2016), and

✉ Zhongyin Xiao
zhyxiao@shu.edu.cn

[1] Key Laboratory of Specialty Fiber Optics and Optical Access Networks, Joint International Research Laboratory of Specialty Fiber Optics and Advanced Communication, Shanghai Institute for Advanced Communication and Data Science, Shanghai University, Shanghai, China

imaging (Lee et al. 2016). In addition, the realization of dynamic MM is one of the most significant goals for MM study. With regard to the MMs converters, most of them have been researched in the dual band, multi-band or broad band (Tang et al. 2016; Ding et al. 2014; Xia et al. 2017; Wen and Zheng 2014). However, in term of the above mentioned works, there are few relevant works being studied on the controlled converter. Actually, the dynamic responses materials, such as GeSbTe (Mkhitaryan et al. 2017), graphene (Zhao et al. 2016), semiconductors (Han et al. 2008), and vanadium dioxide (VO_2) (Shin et al. 2016), can be used to realize the dynamic and flexible modulation. Nevertheless, as an artificial material, the MMs structures can achieve the dynamic modulation easily for THz waves. Recently, there are a few attempts to the realization of tunable polarization conversion. For instance, the dynamic polarization converter with graphene sheets is demonstrated by Yu et al. (Yu et al. 2016) in the THz region. And the proposed device can switch dynamically the polarization state of the incident wave including linear-to-linear, linear-to-circular and linear-to-elliptical polarization state. At present, the thermally controlled MM structure has also been researched. The VO_2, a phase transition material, has been presented theoretically for achieving the thermal modulation of the linear polarization conversion (Lv et al. 2016). Generally, the VO_2 film undergoes a phase transition from insulator to metal under varying temperatures (Jepsen et al. 2006). This dramatic change of the VO_2 film has prompted the development of many novel applications in MMs, such as switches, modulators, and tunable devices. In addition, in order to control the polarization state, researchers have tried their best to study the reflective MM structures. For examples, asymmetric cross-shaped resonator (Zhang et al. 2016a, b) and the anisotropic MM (Zhao et al. 2016) have been used to realize the broadband polarization converter. But the converters are not involved in the aspects of tunable characteristics of the polarization conversion. From these perspectives, the reflective polarization conversion devices still need to be developed.

In this article, a tunable reflective polarization converter is proposed in the THz region. The converter is composed of the hybrid material, a gold film and a dielectric substrate. Numerical results show that a polarization conversion ratio (PCR) above 90% can be obtained from 2.10 to 5.03 THz for both linearly and circularly polarized incident waves. Moreover, the polarization conversion performance of metamaterial structure is sensitive to the incident angles. The related ellipticity and the polarization rotation azimuth angle can verify the polarization purity in term of polarization conversion. In addition, the simulated results show that the proposed converter can realize thermal modulation for the polarization conversion. And the distributions of surface currents are analyzed to illustrate the modulation characters. It is worth mentioning that the proposed hybrid metamaterial can be used in the tunable THz polarization devices.

2 Structure design

The designed polarization converter consists of a hybrid layer, a gold (Au) film and a dielectric spacer. The metallic material is dealt with in the Drude model which means the effective permittivity of metals in the terahertz spectral region is given by $\varepsilon(\omega) = 1 - \omega_p^2/\omega(\omega + i\omega_c)$ (Linden et al. 2004), where ω_p is the plasma frequency, and ω_c is the collision frequency. For the metallic gold, the parameters are $\omega_p = 2\pi \times 2175$ THz and $\omega_c = 2\pi \times 4.35$ THz. The lossy polyimide substrate is chosen as dielectric space and the relative dielectric constant of polyimide is 3.5 (Zhang et al. 2016a, b). The hybrid layer is

composed of the I-shaped resonator and VO_2 film. The complex properties of VO_2 film can be expressed further with the Bruggeman effective model, given as follows (Lv et al. 2016)

$$\varepsilon(VO_2) = \frac{1}{4}\left\{\varepsilon_d(2-3V) + \varepsilon_m(3V-1) + \sqrt{\left[\varepsilon_d(2-3V) + \varepsilon_m(3V-1)^2 + 8\varepsilon_d\varepsilon_m\right]}\right\} \quad (1)$$

In this formula, ε_d is the dielectric constants of the insulating, ε_m denotes the dielectric constants of the VO_2 films, and V represents the volume fraction of the metallic regions. In the simulations, the relative permittivity for the VO_2 film is taken as 9 and the conductivity of VO_2 film (σ_{VO_2}) is 200 S/m at the temperature about 25 °C (Lv et al. 2016; Wen et al. 2012; Zhu et al. 2013). In order to understand the reflected waves preferably, the $r_{yy} = E_{yr}/E_{yi}$, $r_{xy} = E_{xr}/E_{yi}$, $r_{xx} = E_{xr}/E_{xi}$, and $r_{yx} = E_{yr}/E_{xi}$ are defined as the different reflection coefficients, respectively. The proposed converter is analyzed by the software of CST Microwave Studio. The schematic diagram and geometric parameters of the polarization converter unit cell are given in Fig. 1. Figure 1a–c show the front view, right view and perspective view of the proposed structure, respectively. The lattice constants along x and y directions are both $p = 30$ μm. The thickness of polyimide is $d = 10$ μm. And the other parameters are given as follows: $w = 4.75$ μm, $g = 1$ μm, $L_1 = 12$ μm, $L_2 = 24.25$ μm, $t = 0.2$ μm.

3 Results and discussion

Figure 2 shows the simulated values of the reflectance when the incidence waves are along the vertical incident direction. First look at the Fig. 1a, it is clear that the $|r_{yx}|$, a kind of cross-polarization reflection coefficient, is equal to $|r_{xy}|$. Similarly, the values of $|r_{xx}|$ are also equivalent to $|r_{yy}|$. Therefore, the hybrid metamaterial is a polarization insensitive periodic structure, meaning that no matter the incident wave is the x-polarized wave or the y-polarized wave, the simulated results are the same. In this case, we only choose the y-polarized incident wave to develop our analysis. As Fig. 2a shown, the reflection coefficient $|r_{xy}|$ is more than 0.88 in a broad frequency region from 2.10 to 5.03 THz. At the same time, the reflection coefficient $|r_{yy}|$ is under 0.30 for the y-polarized incidence wave. It is worth noting that the curves of reflection coefficients have three distinct

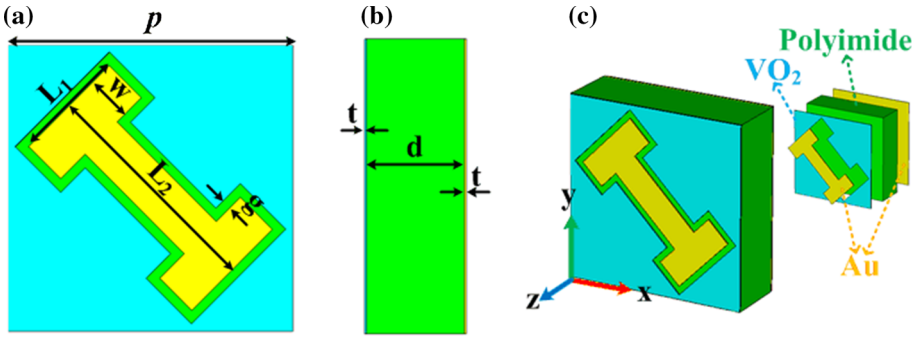

Fig. 1 Schematic diagram and geometric parameters of the polarization converter unit cell. **a** The front view, **b** the right view, and **c** the perspective view

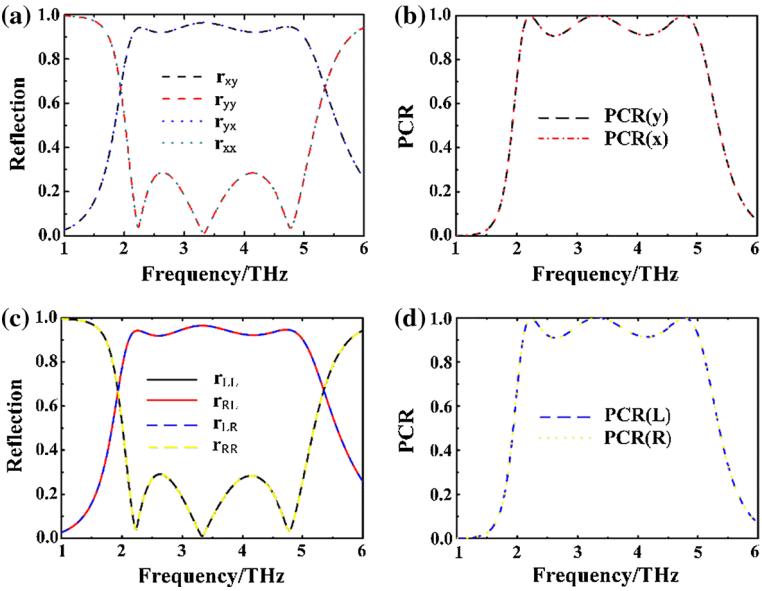

Fig. 2 **a** Simulated reflection spectra, and **b** PCR for linearly polarized wave. **c** Simulated reflection spectra, and **d** PCR for circularly polarized wave

resonant peaks at 2.23, 3.32, and 4.78 THz, respectively. Especially the value of $|r_{yy}|$ is nearly zero at the three resonance points and it reveals that there is only x-polarized component of the total reflected waves. In other words, nearly total y-polarized wave is converted to its cross-polarization wave after reflection effect. In order to understand the polarization conversion, the polarization conversion ratio (PCR) can be defined as $PCR(y) = |r_{xy}|^2/(|r_{yy}^{|2} + |r_{xy}|^2)$ (Jepsen et al. 2006). Figure 2b represents the values of PCR for the linearly polarized wave. The PCR more than 90% is achieved in a broad frequency range from 2.10 THz to 5.03 THz. Especially, the value of PCR reaches near unity around the resonant frequency points due to the phenomenon of electromagnetic resonance.

What's more, we calculated the reflection coefficients under the circularly polarized incidence. The reflection coefficients $|r_{RL}| = E_{Rr}/E_{Li}$, $|r_{LL}| = E_{Lr}/E_{Li}$, $|r_{LR}| = E_{Lr}/E_{Ri}$ and $|r_{RR}| = E_{Rr}/E_{Ri}$, are define as the different reflection coefficients respectively. As Fig. 2c, d shown, the reflection coefficients under the circularly polarized wave excitation are equivalent to the corresponding reflection coefficients under the linearly polarized incident wave, namely $|r_{RL}| = |r_{LR}| = |r_{xy}| = |r_{yx}|$ and $|r_{LL}| = |r_{RR}| = |r_{xx}| = |r_{yy}|$. In addition, the PCR remains the same for linearly and circularly polarized incident wave. Therefore, the simulation results under the linearly polarized wave or the circularly polarized wave are the same. Based on the above analysis, we find out that the proposed structure can act as a reflection convertor under the linearly or circularly polarized incidences.

We also calculated the results under different incident angles when the y-polarized wave propagates along the − z direction. First look at the reflection coefficients shown in Fig. 3a, the solid lines represent the cross-polarized reflection coefficients and the dashed lines with the same color stand for the corresponding co-polarized reflection coefficients. With the increase of the incident angles, the phenomenon of the polarization conversion becomes weaker and weaker. Because the value of $|r_{xy}|$ gets smaller and smaller while the coefficients of $|r_{yy}|$ change bigger and bigger. From Fig. 3b, we can obviously find out that

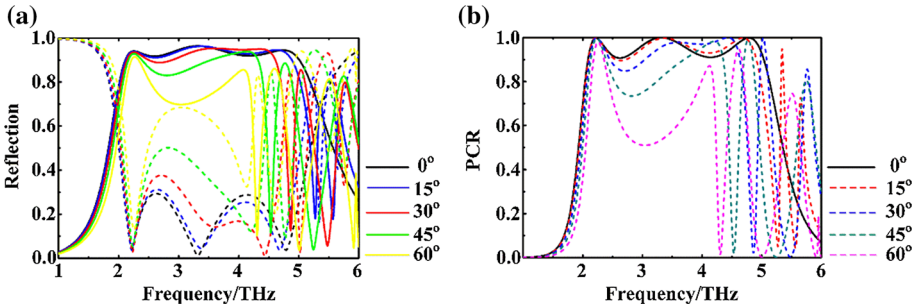

Fig. 3 **a** The reflection coefficients and **b** PCR under different incident angles with y-polarized incidence

even more resonant frequencies come out, the bandwidth of the PCR decrease greatly with the increase of the incident angles. In the frequency band from 2.2 to 4.48 THz, there only exist two resonant points under oblique incidence and the value of the PCR drops less than 90% with the increase of the incident angles. Especially when the incident angle is larger than 45°, the simulation results are unacceptable. Therefore, the simulation data indicate that the hybrid metamaterial is sensitive to the incident angles. Only incident structure normally can we get the best results.

To better understand the polarization conversion, polarization azimuth angle θ and ellipticity η for the y-polarized incident wave are also calculated. The polarization azimuth angle θ and ellipticity η can be described as (Jepsen et al. 2006; Zhao and Cheng 2017):

$$\theta = \frac{1}{2}\arctan\left(\frac{2p_r\cos(\varphi_r)}{1-|p_r|^2}\right) \tag{2}$$

$$\eta = \frac{1}{2}\arcsin\left(\frac{2p_r\sin(\varphi_r)}{1+|p_r|^2}\right) \tag{3}$$

where $p_r = |r_{xy}|/|r_{yy}|$ and $\varphi_r = \arg(r_{xy}) - \arg(r_{yy})$. The θ is the angle between the polarization planes of the reflected and incident waves, while the η denotes the polarization state of the reflected wave. When $\eta = 0°$, the reflected wave is still linearly polarized but the polarization plane has an angle of θ with respect to the incident wave. Therefore, the pure

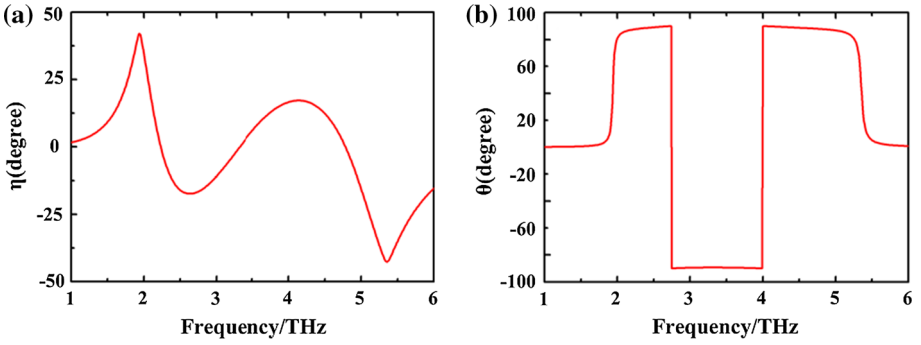

Fig. 4 **a** The ellipticity η, and **b** the polarization azimuth angles θ for y-polarization

linearly polarized wave can be obtained when $\eta = 0°$ and $\theta = \pm 90°$. The calculate results for η and θ are shown in Fig. 4a, b.

From Fig. 4a, it can be clearly seen that the ellipticity η of the y-polarized incident wave is less than 20° from 2.10 to 5.03 THz and the result shows that a near linear polarization state is maintained. Especially, the value of η is in the vicinity of zero at three resonance points, indicating a pure linearly polarized wave in reflection. Furthermore, the value of θ is in the vicinity of $\pm$ 90° from 2.10 to 5.03 THz. At the same time, θ is near $-$ 90° in the frequency range of 2.74–3.99 THz. This can be verified from Fig. 4b. Therefore, it can be concluded that the y-polarized wave can be converted to the x-polarized wave at three resonance points about 2.23, 3.325 and 4.78 THz respectively.

The polyimide material has a low thermal conductivity and a relatively high specific heat (Narayana et al. 2013). Thus, the polyimide has high thermal stable performance (Dai et al. 2015). And the gold can be taken as lossy metal with the conductivity of 4.561×10^7 S/m. So, effect of the temperature on the gold layer is also neglected (Lv et al. 2016). To better reveal the tunable reflective polarization conversion, the conductivities of VO_2 films are researched at different temperatures. Generally, the various temperatures have enormous impact on the conductivities of VO_2 (Jepsen et al. 2006; Wen et al. 2010). The characteristics of VO_2 film will be changed with the conductivity tuning. The VO_2 film with various conductivities can exhibit a dynamic insulator–metal phase transition which can be triggered thermally (Wen et al. 2010; Zhao et al. 2012; Liu et al. 2012). Furthermore, the VO_2 shows an insulating state when the (σ_{VO_2}) is smaller than 200 S/m. However, when the value of (σ_{VO_2}) is greater than 10^5 S/m, the film can be regarded as a metallic state. By the way, the value conductivity of VO_2 film is 200 S/m with the temperature risen to 25 °C. When the temperature is about 85 °C, the VO_2 film conductivity is 10^5 S/m (Lv et al. 2016; Zhao and Cheng 2017). Thus, the VO_2 film can be used as a thermal material. In conclusion, the insulator–metal transition of VO_2 has drawn intense scientific interest for the changing polarization conversion state. The simulated curves of PCR efficiency as the function of conductivities are presented in Fig. 5.

From Fig. 5, the value of PCR is more than 90% from 2.10 to 5.03 THz when the conductivity of VO_2 film is less than 200 S/m. And it can be seen clearly that the PCR efficiency will decrease significantly with the conductivity increasing from 200 to 10^5 S/m. Especially, when the conductivity of VO_2 film increases to 5×10^3 S/m, the PCR efficiency of the converter is above 79% in a broad range from 2.10 to 5.03 THz. While the conductivity is 10^4 S/m, the PCR is only more than 57% in this frequency range. In addition, as the conductivity is swept from 200 S/m to 10^4 S/m, there are also three resonance points. Similarly, when the VO_2 film conductivity reaches 4×10^4 S/m, the PCR is less than 41% and as the conductivity is 10^5 S/m, the PCR is no more than 15%.

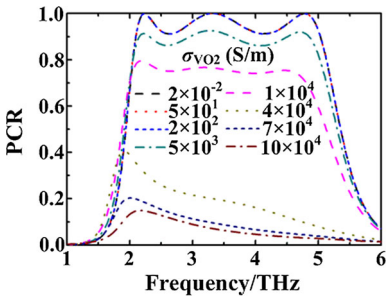

Fig. 5 Simulated polarization conversion ratio curves on the conductivity of VO_2 film

And there is only one the resonance frequency when the conductivity is swept from 4×10^4 to 10^5 S/m. In other words, when the conductivity is 10^5 S/m, the y-polarized wave cannot be converted to the x-polarized wave. Accordingly, the insulator–metal phase transition of VO_2 can change the polarization conversion state. When the property of VO_2 film is insulating state, the hybrid layer allows the wave transmission, leading to the polarization conversion. However, when the character of VO_2 film is regarded as metal state, the hybrid layer will prevent wave transmission, causing no strong polarization conversion effects. Thus, it can be concluded unambiguously that the VO_2 film can induce thermal switching effect of polarization conversion. And it can be used in the adjustable polarization converter.

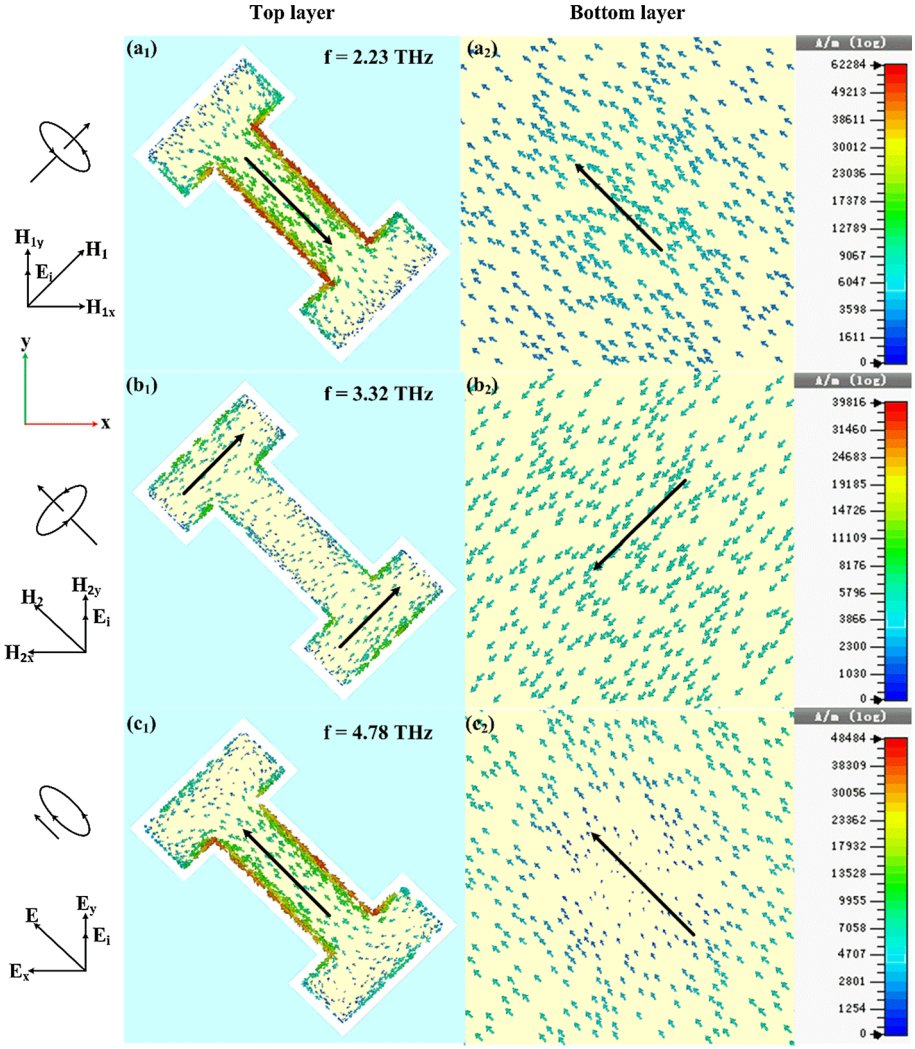

Fig. 6 Simulated distributions of the surface currents of the hybrid metamaterial polarization converter for the y-polarized incident wave at the three resonance points

To further understand the physical mechanism of the polarization conversion, the simulated distributions of the surface currents are drawn in Fig. 6 at the three resonant frequencies of 2.23, 3.32, and 4.78 THz. It is observed that the anti-phase currents between the top and bottom layers at 2.23 and 3.32 THz can be excited by the incident wave. At the resonant frequency 2.23 THz, the direction of the surface current is along the long arm of the I-shaped, which makes the I-shaped resonator equivalent to a cut-wire resonator in this case. However, at the resonant frequency 3.32 THz, the currents flow along the two short arms, hence, the I-shaped structure can be regarded as an electric dipole (Gao et al. 2015; Liu and Giessen 2010). The surface currents along the I-shaped structure are antiparallel to the induced currents on the bottom metallic layer, which generate the magnetic resonance at 2.23 and 3.32 THz. As shown in Fig. 6c_1, c_2, the currents flow along the long arm, which is parallel to the induced currents on the bottom metallic layer. Consequently, the electric resonance can be produced at 4.78 THz (Chen et al. 2014). The magnetic resonance and electric resonance can create the induced magnetic field H_1, H_2, and electric field E, respectively (Gao et al. 2015). In term of the effect of polarization conversion, the H_{1y} and H_{2y} (the component of induced magnetic field H_1 and H_2 along y-direction) (Zhang et al. 2015) are parallel to the incident electric field E_i, which results in the cross-polarization. Nevertheless, the co-polarization will exist because the component H_{1x} and H_{2x} are vertical to the incident electric field E_i. In contrast, the E_x (the component of induced electric field E along x-direction) is vertical to the incident electric field E_i, thus there is cross coupling between E_x and E_i. E_x contributes to the polarization conversion. The component E_y of induced electric field E parallels to the incident electric field E_i, cannot occur at the cross coupling, because the component E_y has the same direction with the incident electric field (Zhang et al. 2015). In other words, the component H_y and E_x can lead to the y-to-x polarization conversion, due to the same direction of the incident electric field (Wen and Zheng 2014; Zhao et al. 2016).

To further understand the physical mechanism of the thermal switching effect the simulated distributions of the surface currents at the conductivities of 10^4 and 10^5 S/m are drawn in Fig. 7. The conductivity of 200, 10^4, and 10^5 S/m at 2.32 THz are taken as examples to describe the thermal excitation. In fact, due to the insulator–metal phase transition of VO_2 film, the structure changes its resonant element (Lv et al. 2016). When the VO_2 film is regarded as the insulating state, corresponding to the resonator of the I-shaped, the top layer is transparent to the incident wave. So, the strong anti-phase currents can be observed when the conductivity is 200 S/m in Fig. 5a_1, a_2. However, the strong anti-phase currents become weak gradually as the conductivity increases (Lv et al. 2016). As the temperature increases, the VO_2 film will transform from the insulator to the metallic state. Meanwhile, due to VO_2 film in a metallic phase, the hybrid layer is regarded as slot metal plate (Lv et al. 2016). The resonator is equivalent to slot metal plate when the conductivity is 10^5 S/m (Zhao and Cheng 2017). The anti-phase current between top and bottom metal layers is existed, but the intensity of the current density is weak in Fig. 7d_1, d_2. Because the metallic VO_2 film cannot allow the transmission of the incident wave, the surface current density is decreased. As the conductivities increased at 3.32 and 4.78 THz, the similar changes of surface currents can be observed. However, when the conductivity is 10^5 S/m, there is only one resonance point. In other words, as the temperature increases, the y-to-x cross-polarization conversion will reduce significantly.

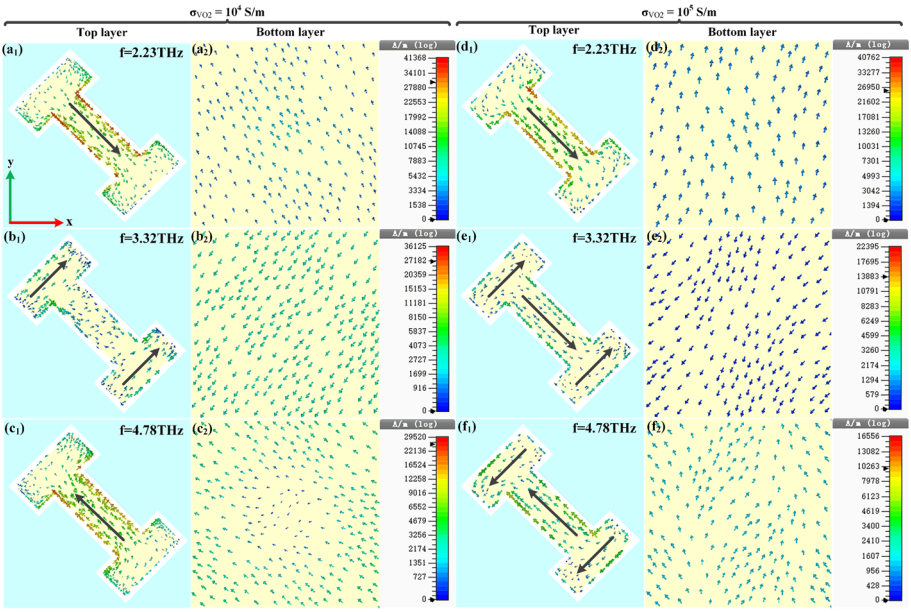

Fig. 7 Simulated distributions of the surface currents of the hybrid metamaterial polarization converter for the y-polarized incident wave at the conductivities of 10^4 and 10^5 S/m

4 Conclusion

The temperature controlled polarization converter based on the hybrid metamaterial structure has been demonstrated in the THz range. The results indicate that the high PCR and the broad bandwidth can be accomplished for the linearly and circularly polarized waves but are sensitive to the incident angles. The proposed converter can also realize dynamic modulation of the polarization conversion by adjusting the conductivity of VO_2 film. In other words, as the temperature increases, the PCR efficiency of the polarization converter changes significantly. In addition, the distributions of surface currents are investigated to explain the characteristic of the polarization conversion. The results are very useful to design novel devices, such as tunable THz devices, thermal detectors, and modulators.

Acknowledgements This work is supported by the National Natural Science Foundation of China (Grant No. 61275070) and Shanghai Natural Science Foundation (Grant No. 15ZR1415900).

References

Chen, H., Wang, J., Ma, H., Qu, S., Xu, Z., Zhang, A., Yan, M., Li, Y.: Ultra-wideband polarization conversion metasurfaces based on multiple plasmon resonances. J. Appl. Phys. **115**(15), 154504 (2014)

Dai, W., Yu, J., Wang, Y., Song, Y., Alam, F.E., Nishimura, K., Lin, C.T., Jiang, N.: Enhanced thermal conductivity for polyimide composites with a three-dimensional silicon carbide nanowire@ graphene sheets filler. J. Mater. Chem. A **3**(9), 4884–4891 (2015)

Ding, J., Arigong, B., Ren, H., Zhou, M., Shao, J., Lin, Y., Zhang, H.: Efficient multiband and broadband cross polarization converters based on slotted L-shaped nanoantennas. Opt. Express **22**(23), 29143–29151 (2014)

Dyachenko, P.N., Molesky, S., Petrov, A.Y., Störmer, M., Krekeler, T., Lang, S., Ritter, M., Jacob, Z., Eich, M.: Controlling thermal emission with refractory epsilon-near-zero metamaterials via topological transitions. Nat. Commun. **7**, 11809 (2016)

Gao, X., Han, X., Cao, W.P., Li, H.O., Ma, H.F., Cui, T.J.: Ultrawideband and high-efficiency linear polarization converter based on double V-shaped metasurface. IEEE Trans. Antennas Propag. **63**(8), 3522–3530 (2015)

Grady, N.K., Heyes, J.E., Chowdhury, D.R., Zeng, Y., Reiten, M.T., Azad, A.K., Taylor, A.J., Dalvit, D.A.R., Chen, H.T.: Terahertz metamaterials for linear polarization conversion and anomalous refraction. Science **340**, 1235399 (2013)

Han, J., Lakhtakia, A., Qiu, C.W.: Terahertz metamaterials with semiconductor split-ring resonators for magnetostatic tunability. Opt. Express **16**(19), 14390–14396 (2008)

Jepsen, P.U., Fischer, B.M., Thoman, A., Helm, H., Suh, J.Y., Lopez, R., Haglund Jr., R.F.: Metal-insulator phase transition in a VO_2 thin film observed with terahertz spectroscopy. Phys. Rev. B **74**(20), 205103 (2006)

Landy, N.I., Sajuyigbe, S., Mock, J.J., Smith, D.R., Padilla, W.J.: Perfect metamaterial absorber. Phys. Rev. Lett. **100**(20), 207402 (2008)

Lee, H., Oh, J.H., Seung, H.M., Cho, S.H., Kim, Y.Y.: Extreme stiffness hyperbolic elastic metamaterial for total transmission subwavelength imaging. Sci. Rep. **6**, 24026 (2016)

Linden, S., Enkrich, C., Wegener, M., Zhou, J., Koschny, T., Soukoulis, C.M.: Magnetic response of metamaterials at 100 Terahertz. Science **306**(5700), 1351 (2004)

Liu, N., Giessen, H.: Coupling effects in optical metamaterials. Angew. Chem. Int. Ed. **49**(51), 9838–9852 (2010)

Liu, M., Hwang, H.Y., Tao, H., Strikwerda, A.C., Fan, K., Keiser, G.R., Wolf, S.A.: Terahertz-field-induced insulator-to-metal transition in vanadium dioxide metamaterial. Nature **487**(7407), 345–348 (2012)

Lu, M., Li, W., Brown, E.R.: Second-order bandpass terahertz filter achieved by multilayer complementary metamaterial structures. Opt. Lett. **36**(7), 1071–1073 (2011)

Lv, T.T., Li, Y.X., Ma, H.F., Zhu, Z., Li, Z.P., Guan, C.Y., Shi, J.H., Zhang, H., Cui, T.J.: Hybrid metamaterial switching for manipulating chirality based on VO_2 phase transition. Sci. Rep. **6**, 23186 (2016)

Mkhitaryan, V.K., Ghosh, D.S., Rudé, M., Canet-Ferrer, J., Maniyara, R.A., Gopalan, K.K., Pruneri, V.: Tunable complete optical absorption in multilayer structures including $Ge_2Sb_2Te_5$ without lithographic patterns. Adv. Opt. Mater. **5**(1), 1600452 (2017)

Narayana, S., Savo, S., Sato, Y.: Transient heat flux shielding using thermal metamaterials. Appl. Phys. Lett. **102**(20), 201904 (2013)

Shin, J.H., Park, K.H., Ryu, H.C.: Electrically controllable terahertz square-loop metamaterial based on VO_2 thin film. Nanotechnology **27**(19), 195202 (2016)

Tang, J., Xiao, Z., Xu, K., Ma, X., Liu, D., Wang, Z.: Cross polarization conversion based on a new chiral spiral slot structure in THz region. Opt. Quantum Electron. **48**(2), 1–11 (2016)

Wang, B.X., Zhai, X., Wang, G.Z., Huang, W.Q., Wang, L.L.: A novel dual-band terahertz metamaterial absorber for a sensor application. J. Appl. Phys. **117**(1), 014504 (2015)

Wen, X., Zheng, J.: Broadband THz reflective polarization rotator by multiple plasmon resonances. Opt. Express **22**(23), 28292–28300 (2014)

Wen, Q.Y., Zhang, H.W., Yang, Q.H., Xie, Y.S., Chen, K., Liu, Y.L.: Terahertz metamaterials with VO_2 cut-wires for thermal tunability. Appl. Phys. Lett. **97**(2), 021111 (2010)

Wen, Q.Y., Zhang, H.W., Yang, Q.H., Chen, Z., Long, Y., Jing, Y.L., Lin, Y.M., Zhang, P.X.: A tunable hybrid metamaterial absorber based on vanadium oxide films. J. Phys. D Appl. Phys. **45**(23), 235106 (2012)

Xia, R., Jing, X., Zhu, H., Wang, W., Tian, Y., Hong, Z.: Broadband linear polarization conversion based on the coupling of bilayer metamaterials in the terahertz region. Opt. Commun. **383**, 310–315 (2017)

Yu, X., Gao, X., Qiao, W., Wen, L., Yang, W.: Broadband tunable polarization converter realized by graphene-based metamaterial. IEEE Photonics Technol. Lett. **28**(21), 2399–2402 (2016)

Zhang, L., Zhou, P., Chen, H., Lu, H., Xie, J., Deng, L.: Broadband and wide-angle reflective polarization converter based on metasurface at microwave frequencies. Appl. Phys. B **120**(4), 617–622 (2015)

Zhang, L., Zhou, P., Lu, H., Zhang, L., Xie, J., Deng, L.: Realization of broadband reflective polarization converter using asymmetric cross-shaped resonator. Opt. Mater. Express **6**(4), 1393–1404 (2016a)

Zhang, J., Wang, G., Zhang, B., He, T., He, Y., Shen, J.: Photo-excited broadband tunable terahertz metamaterial absorber. Opt. Mater. **54**, 32–36 (2016b)

Zhao, J., Cheng, Y.: A high-efficiency and broadband reflective 90° linear polarization rotator based on anisotropic metamaterial. Appl. Phys. B **122**(10), 255 (2016)

Zhao, J.C., Cheng, Y.Z.: Ultra-broadband and high-efficiency reflective linear polarization convertor based on planar anisotropic metamaterial in microwave region. Opt. Int. J. Light Electron Opt. **136**, 52–57 (2017)

Zhao, Y., Lee, H.J., Zhu, Y., Nazari, M., Chen, C., Wang, H., Bernussi, A., Holtz, M., Fan, Z.: Structural, electrical, and terahertz transmission properties of VO_2 thin films grown on c-, r-, and m-plane sapphire substrates. J. Appl. Phys. **111**(5), 053533 (2012)

Zhao, X., Yuan, C., Zhu, L., Yao, J.: Graphene-based tunable terahertz plasmon-induced transparency metamaterial. Nanoscale **8**(33), 15273–15280 (2016)

Zhu, Y., Vegesna, S., Zhao, Y., Kuryatkov, V., Holtz, M., Fan, Z., Saed, M., Bernussi, A.A.: Tunable dual-band terahertz metamaterial bandpass filters. Opt. Lett. **38**(14), 2382–2384 (2013)